Neurobiology of Disease 138 (2020) 104794

Contents lists available at ScienceDirect

Neurobiology of Disease

journal homepage: www.elsevier.com/locate/ynbdi

Multielectrode array analysis of EEG biomarkers in a mouse model of Fragile X Syndrome

Carrie R. Jonak[a], Jonathan W. Lovelace[c], Iryna M. Ethell[a,b], Khaleel A. Razak[b,c], Devin K. Binder[a,b,*]

[a] Division of Biomedical Sciences, School of Medicine, University of California, Riverside, United States of America
[b] Neuroscience Graduate Program, University of California, Riverside, United States of America
[c] Department of Psychology, University of California, Riverside, United States of America

ARTICLE INFO

Keywords:
Fragile X syndrome
Autism
Auditory cortex
Sensory hypersensitivity
EEG
Multielectrode array
Gamma power

ABSTRACT

Fragile X Syndrome (FXS) is a leading known genetic cause of intellectual disability with symptoms that include increased anxiety and social and sensory processing deficits. Recent EEG studies in humans with FXS have identified neural oscillation deficits that include increased resting state gamma power, increased amplitude of auditory evoked potentials, and reduced inter-trial phase coherence of sound-evoked gamma oscillations. Identification of comparable EEG biomarkers in mouse models of FXS could facilitate the pre-clinical to clinical therapeutic pipeline. However, while human EEG studies have involved 128-channel scalp EEG acquisition, no mouse studies have been performed with more than three EEG channels. In the current study, we employed a recently developed 30-channel mouse multielectrode array (MEA) system to record and analyze resting and stimulus-evoked EEG signals in WT *vs. Fmr1* KO mice. Using this system, we now report robust MEA-derived phenotypes including higher resting EEG power, altered event-related potentials (ERPs) and reduced inter-trial phase coherence to auditory chirp stimuli in *Fmr1* KO mice that are remarkably similar to those reported in humans with FXS. We propose that the MEA system can be used for: (i) derivation of higher-level EEG parameters; (ii) EEG biomarkers for drug testing; and (ii) mechanistic studies of FXS pathophysiology.

1. Introduction

Fragile X Syndrome (FXS) is the most common genetic cause of intellectual disability with symptoms that overlap with autism spectrum disorders (ASD) (Crawford et al., 2001). FXS is caused by a mutation in the *Fragile X Mental Retardation 1 (Fmr1)* gene and a loss of Fragile X Mental Retardation Protein (FMRP) (Yu et al., 1991). FMRP is an RNA-binding protein that regulates synaptic function through regulation of protein translation (Darnell et al., 2011). Symptoms associated with FXS include increased anxiety, repetitive behaviors, social communication deficits, delayed language development and abnormal sensory processing (Abbeduto and Hagerman, 1997; Berry-Kravis, 2002; Hagerman et al., 2009; Miller et al., 1999; Musumeci et al., 1999; Roberts et al., 2001; Sabaratnam et al., 2001; Sinclair et al., 2017c; Van der Molen et al., 2010; Wisniewski et al., 1991). Abnormal sensory processing in FXS includes hypersensitivity and reduced habituation to repeated sensory stimuli (Castrén et al., 2003; Schneider et al., 2013).

Auditory processing deficits are common in both humans with FXS (Castrén et al., 2003; Ethridge et al., 2016; Schneider et al., 2013; Van der Molen and Van der Molen, 2013a) and *Fmr1* knockout (KO) mice (Lovelace et al., 2016, 2018; Rotschafer and Razak, 2013, 2014; Wen et al., 2018), a mouse model of FXS (Bernardet and Crusio, 2006). Recent EEG recordings from humans showed altered cortical oscillatory activity that may contribute to sensory hypersensitivity and social communication deficits in FXS (Ethridge et al., 2017; Wang et al., 2017). Gamma frequency power was enhanced in humans with FXS compared to healthy controls (Wang et al., 2017). When neural oscillations were induced with auditory "chirp" stimuli, inter-trial phase coherence (phase-locking) was reduced in humans with FXS, particularly at gamma frequencies (Ethridge et al., 2017). The non-phase locked single-trial power was, however, enhanced in FXS. These results suggest that enhanced background gamma oscillations ('gamma noise') may contribute to hypersensitivity and interfere with stimulus-evoked synchronization in FXS. Importantly, these phenotypes were correlated with parent reports of social communication deficits and hypersensitive sensory responses suggesting clinical relevance of the EEG measures (Ethridge et al., 2017).

Identification of comparable biomarkers in humans and validated

* Corresponding author at: Division of Biomedical Sciences, University of California, 900 University Avenue, Riverside, CA 92521, United States of America.
E-mail address: dbinder@ucr.edu (D.K. Binder).

https://doi.org/10.1016/j.nbd.2020.104794
Received 4 November 2019; Received in revised form 27 January 2020; Accepted 5 February 2020
Available online 06 February 2020

animal models is a critical step in facilitating pre-clinical to clinical therapeutic pipelines to treat neurodevelopmental disorders (Berry-Kravis et al., 2018). In an initial set of studies, we recorded EEGs in awake, freely moving *Fmr1* KO mice using similar stimuli as in the human studies. We found remarkably similar phenotypes in frontal and auditory cortex of the *Fmr1* KO mice including enhanced resting state gamma power and reduced inter-trial phase coherence (ITPC) to auditory "chirp" stimuli (Lovelace et al., 2018). However, these initial studies were done with three epidural screw electrodes (frontal, auditory, and occipital). Thus, a potentially important technical difference between the human studies and our mouse studies is that we have used different methods to collect and analyze EEG data between species. The data collected from humans with FXS utilized large EEG arrays with 128 leads, which allows spatial mapping of oscillations, examination of the spread of neural excitation across cortex, and powerful principal component analysis of multiple channels. Our recordings with 3 cortical electrodes used a common ground in the occipital lobe, and recording electrodes in the frontal and auditory cortices, resulting in 2 channels of derived data. Because of this electrode limitation in mice in our initial studies, the spatial representation of oscillations was limited, which could cause us to miss important alterations in oscillations that were revealed in human data, especially amplitude and frequency coupling across regions. For these reasons, it is desirable to align mouse electrophysiology data acquisition methods to more closely match those used in human studies.

To address these issues, we have developed and applied multi-electrode array (MEA) analysis in mice (Jonak et al., 2018). Our system involves stable chronic *in vivo* implantation of a planar multielectrode array (MEA) on the surface of the mouse skull and enables low-noise 30-channel simultaneous EEG, which can then be used for resting and stimulus-evoked EEG acquisition in awake, freely moving mice (Jonak et al., 2018). For auditory stimulation, we used paradigms analogous to those used in human studies (Ethridge et al., 2017) and identical to those previously reported in the 2-channel data (Lovelace et al., 2018). Using this system, we now report MEA-derived EEG phenotypes in *Fmr1* KO mice that are similar to those observed in humans and provide novel insights into abnormal sensory processing in FXS. In particular, we demonstrate robust MEA-derived phenotypes of altered resting EEG power, event-related potentials (ERPs), single-trial and train-related EEG power, and inter-trial phase coherence (ITPC) to auditory chirp stimuli in *Fmr1* KO mice.

2. Methods

2.1. Animals

Fmr1 KO (B6.129P2-*Fmr1*^{tm1Cgr}/J, stock #003025) (Bakker et al., 1994) and C57BL/6J WT (stock #000664) mice were obtained from Jackson Laboratories at 8 weeks of age and were housed in our animal facility before and after surgical procedures. Animals were maintained under a 12-hour light/dark cycle and were provided irradiated rodent diet (PicoLab, 5053) and water *ad libitum*. All experiments were performed with approval from the University of California Animal Care and Use Committee and in accordance with the National Institutes of Health Animal Care and Use Guidelines. EEG recordings were obtained from 11 *Fmr1* KO and 10 WT mice. Males between 2 and 3 months of age were used for all EEG recordings.

2.2. MEA implantation

Mice were anesthetized with isoflurane inhalation (0.2–0.5%) and given an i.p. injection cocktail of ketamine 80 mg/kg (Zoetis,10004027) and xylazine 10 mg/kg (Bimeda, 1XYL003). Mice were aseptically prepared for surgery and secured in a stereotaxic apparatus. Artificial tear ointment (Henry Schein, 01169568321) was applied to the eyes to prevent drying. Toe pinch reflex was used to measure anesthetic depth throughout the surgery, and supplemental doses of K/X were administered as needed. Once the mouse was anesthetized, a midline sagittal incision was made along the scalp to expose the skull. A cotton-tip applicator was used to remove the periosteum from the skull and to clean skull with saline. A surgical marker was used to mark bregma and positions of three screws. A dental drill was used to drill 1 mm diameter holes in the skull overlying the left frontal cortex, left cerebellum and right cerebellum. Screws (PlasticsOne, 00-96 X 1/16) were advanced into drilled holes until secure; special care was taken not to advance the screws beyond the point of contact with the dura. The probe grounding wire was placed in the nuchal musculature and the probe was placed on the skull surface carefully aligning the "+" in the center of the probe with bregma. Saline was added to the top of the probe to aid in adherence to the skull surface and allowed to dry. A 4-0 silk tie was used to secure the probe ribbon between the two cerebellum screws and Teflon/plastic wrap was placed on top of the probe. Dental cement (Kuraray, 3382KA) was applied around the screws, on the base of the cotton-tip applicator post, and the Teflon/plastic wrap covering the probe. Waterproof medical tape was used to secure the cotton-tip applicator to the probe connector. Triple antibiotic was applied along the edges of the dental cement followed by a subcutaneous injection of buprenorphine 0.1 mg/kg (Reckitt & Colman, 5053624). Mice were placed on a heating pad to aid in recovery from anesthesia and additional doses of buprenorphine were administered every 6–8 h for continuous analgesia during the first 48 h after surgery. Mice were then individually housed with nesting material (Ancare, NES3600) for environmental enrichment, returned to the vivarium and monitored daily until the day of EEG recordings. Animals were recorded between 2 and 4 days after surgery.

2.3. Acoustic stimulation

All experiments were conducted in a sound-attenuated chamber lined with anechoic foam (Gretch-Ken Industries, Oregon). Acoustic stimuli were generated using RPVDSEX software and RZ6 hardware (Tucker Davis Technologies, FL) and presented through a free-field speaker (MF1 Multi-Field Magnetic Speaker; Tucker-Davis Technologies, FL) located 12 in. directly above the cage. Sound pressure level (SPL) was modified using programmable attenuators in the RZ6 system. The speaker output was ~70 dB SPL at the floor of the recording chamber with fluctuation of ± 3 dB for frequencies between 5 and 35 kHz as measured with a ¼ inch Bruel & Kjaer microphone.

After 5 min of EEG recording without any sound (resting EEG), we first presented broadband noise to record auditory event-related potentials (ERPs) to identify various components (P1, N1, P2) for comparison to previous animal (Lovelace et al., 2018; Lovelace et al., 2016; Wen et al., 2019) and human (Castrén et al., 2003; Van der Molen et al., 2012) studies. ERPs were recorded in response to trains of broadband noise with each train consisting of 10 repetitions (1 Hz repetition rate). Each noise stimulus was 100 ms in duration, with a 5 ms rise/fall time and was presented at 70 dB SPL. The inter-train interval was 8 s. The total duration of broadband stimuli was 30 min.

Second, we used an acoustic stimulation paradigm that has been used in humans with FXS to enhance translational relevance. Ethridge et al. (2017) used a chirp-modulated tone (henceforth, 'chirp') to induce synchronized oscillations in their EEG recordings (Ethridge et al., 2017). The chirp stimulus used here was broadband noise whose amplitude was modulated by a sinusoid with linearly increasing frequencies from 1 to 100 Hz (Artieda et al., 2004; Pérez-Alcázar et al., 2008; Purcell et al., 2004). Each stimulus was 2 s in duration, and the depth of modulation was 100%. To avoid onset responses contaminating phase locking to the amplitude modulation of the chirp, the stimulus was ramped in sound level from 0 to 100% over 1 s (rise time) which then smoothly transitioned into chirp modulation of the noise. Chirp trains were presented 300 times each with a random inter-chirp interval between 1 and 1.5 s. The total duration of chirp stimuli was

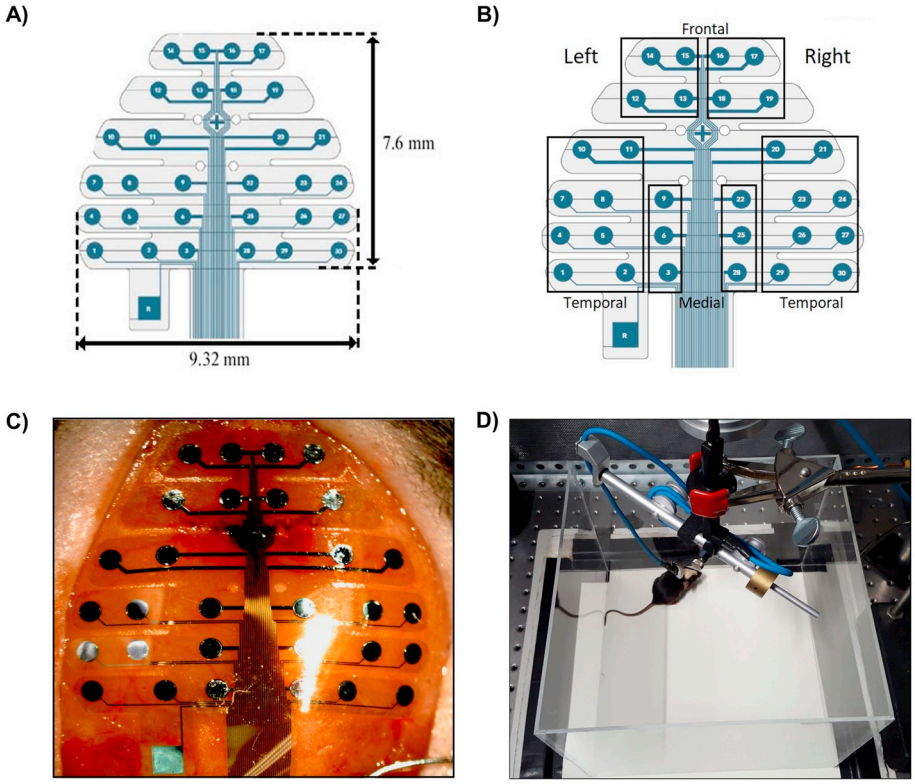

Fig. 1. A. Schematic of multielectrode array probe. **B.** Division into six regions (left and right frontal, temporal, and medial). **C.** MEA probe on mouse skull surface *in situ*. Note that the "+" is situated over bregma. **D.** Freely moving mouse connected to MEA recording apparatus.

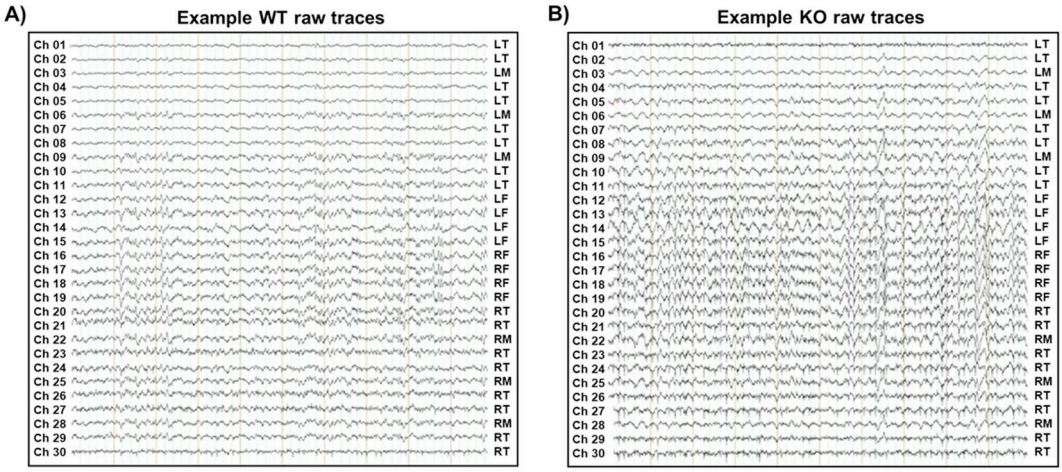

Fig. 2. Example of resting MEA EEG obtained from WT **(A)** and *Fmr1* KO **(B)** mice. Note higher amplitude and frequency in the *Fmr1* KO EEG traces. LT = left temporal; LM = left medial; LF = left frontal; RT = right temporal; RM = right medial; RT = right temporal.

25 min. The chirp facilitates a rapid measurement of transient oscillatory entrainment (delta to gamma frequency range) to auditory stimuli of varying frequencies and can be used to compare oscillatory responses in different groups in clinical and pre-clinical settings (Purcell et al., 2004). Inter-trial phase coherence analysis (phase locking factor) (Tallon-Baudry et al., 1996) can then be used to determine the ability of neural generators to synchronize oscillations to the frequencies present in the repeated stimulus.

2.4. Electrophysiology

Resting and auditory ERP recordings were obtained using the SmartBox (NeuroNexus) from awake and freely moving mice (Jonak et al., 2018). A headstage and tether was connected to the probe post of the mouse skull (implanted during surgery) under brief isoflurane anesthesia. The mouse was then placed inside a grounded Faraday cage after recovery from isoflurane. This tether was then connected to a commutator located directly above the cage. Mice were then allowed to habituate to being connected to the tether for 20 min before EEG recordings were obtained.

The SmartBox acquisition system was connected to the commutator to which the animal was attached. Acquisition hardware was set to lower (0.5 Hz) and upper (500 Hz) filters and data were sampled at a rate of 1250 Hz. Sound delivery was synchronized with EEG recordings using a TTL pulse to mark the onset of each sound in a train. Five minutes of resting EEG was recorded in which no auditory stimuli were

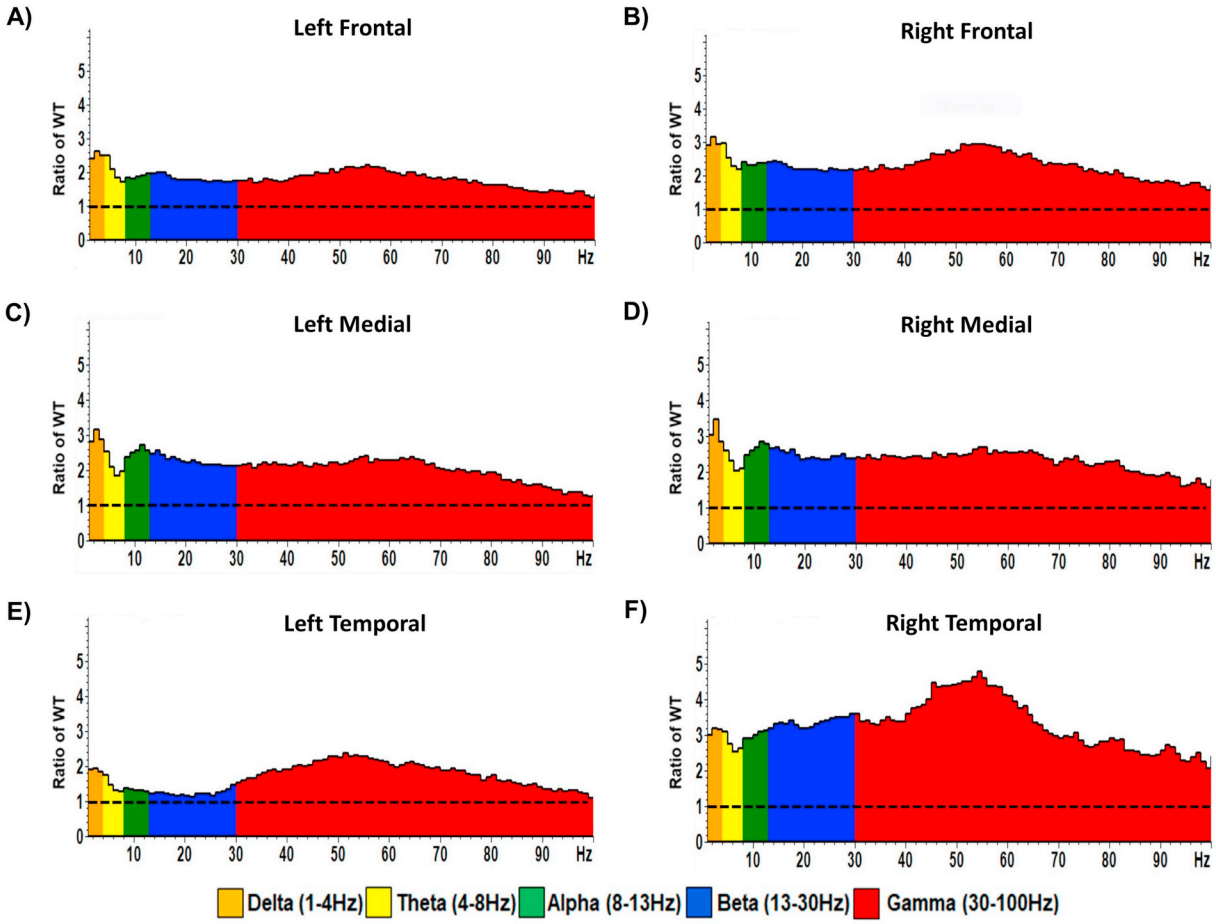

Fig. 3. Ratio of *Fmr1* KO to WT EEG power across frequency bands for distinct brain regions **(A–F)**. Five minutes of resting EEG data from various indicated brain regions was recorded and FFT analysis was done to determine spectral power. Values above 1 indicate higher EEG power in *Fmr1* KO compared with WT mice.

presented. This was followed by ERP recordings in response to trains of broadband noise and chirp stimuli. After these experiments were completed, mice were euthanized.

2.5. Data analyses

Data analyses were done using a combination of Analyzer 2.1 (Brain Vision Inc.), MATLAB, and SPSS. Data were extracted from the Smartbox files and saved in a file format compatible with Analyzer 2.1 software. Data were first down sampled to 625 Hz and a 60 Hz notch filter was used. EEG artifacts were removed using a semi-automatic procedure in Analyzer 2.1 for all recordings. Less than 20% of data were rejected due to artifacts from any single mouse.

Resting (no auditory stimulus) EEG data were divided into 1 second segments and Fast Fourier Transforms (FFT) was run on each segment using 0.5 Hz bins and then average power ($\mu V/Hz^2$) was calculated for each mouse from 1 to 100 Hz. Power was then further binned into standard frequency bands: Delta (1–4 Hz), Theta (4–8 Hz), Alpha (8–13 Hz), Beta (13–30 Hz), and Gamma was divided into "Low Gamma" (30–55 Hz), and "High Gamma" (65–100 Hz).

Single ERP peak analysis was done by obtaining average traces across the first response of all BBN trains (total of 200 trials). Peaks were determined by pre-defined time windows after stimulus onset: P1 (10–30 ms), N1 (30–75 ms), and P2 (75–150 ms).

Two different measures of power were used to analyze single ERP responses as well as responses throughout trains of BBN. Event-related power of single ERP responses was calculated by taking the average trace from the first response (window is ± 500 ms from sound onset) in each of the 1 Hz trains (a total of 200 repetitions) and performing Morlet Wavelet deconvolution using power density ($\mu V^2/Hz$) on the average trace. This same procedure was also used to determine event-related power during entire 1 Hz trains of BBN as well, with windows adjusted to encompass the entire train.

Chirp trains were analyzed using Morlet wavelet analysis. The trains were segmented into 2-second windows during the chirp stimulation. EEG traces were processed with Morlet wavelets from 1 to 100 Hz using complex number output (voltage density, μV/Hz) for inter-trial phase coherence (ITPC) calculations, and power density ($\mu V^2/Hz$) for phase locked power (PL power) calculations and baseline corrected non-phase locked single-trial power (induced power). Wavelets were run with a Morlet parameter of 10 as this gave the best frequency/power discrimination. This parameter was chosen since studies in humans found most robust difference around 40 Hz, where this parameter is centered (Ethridge et al., 2017).

To measure phase synchronization at each frequency across trials, inter-trial phase coherence (ITPC) was calculated. The equation used to calculate ITPC is:

$$ITPC(f,t) = \frac{1}{n}\sum_{k=1}^{n}\frac{F_k(f,t)}{|F_k(f,t)|}$$

where f is the frequency, t is the time point, and k is trial number. Thus, $F_k(f,t)$ refers to the complex wavelet coefficient at a given frequency and time for the kth trial. There were no less than 275 chirp trials (out of 300) for any given mouse after segments containing artifacts were rejected.

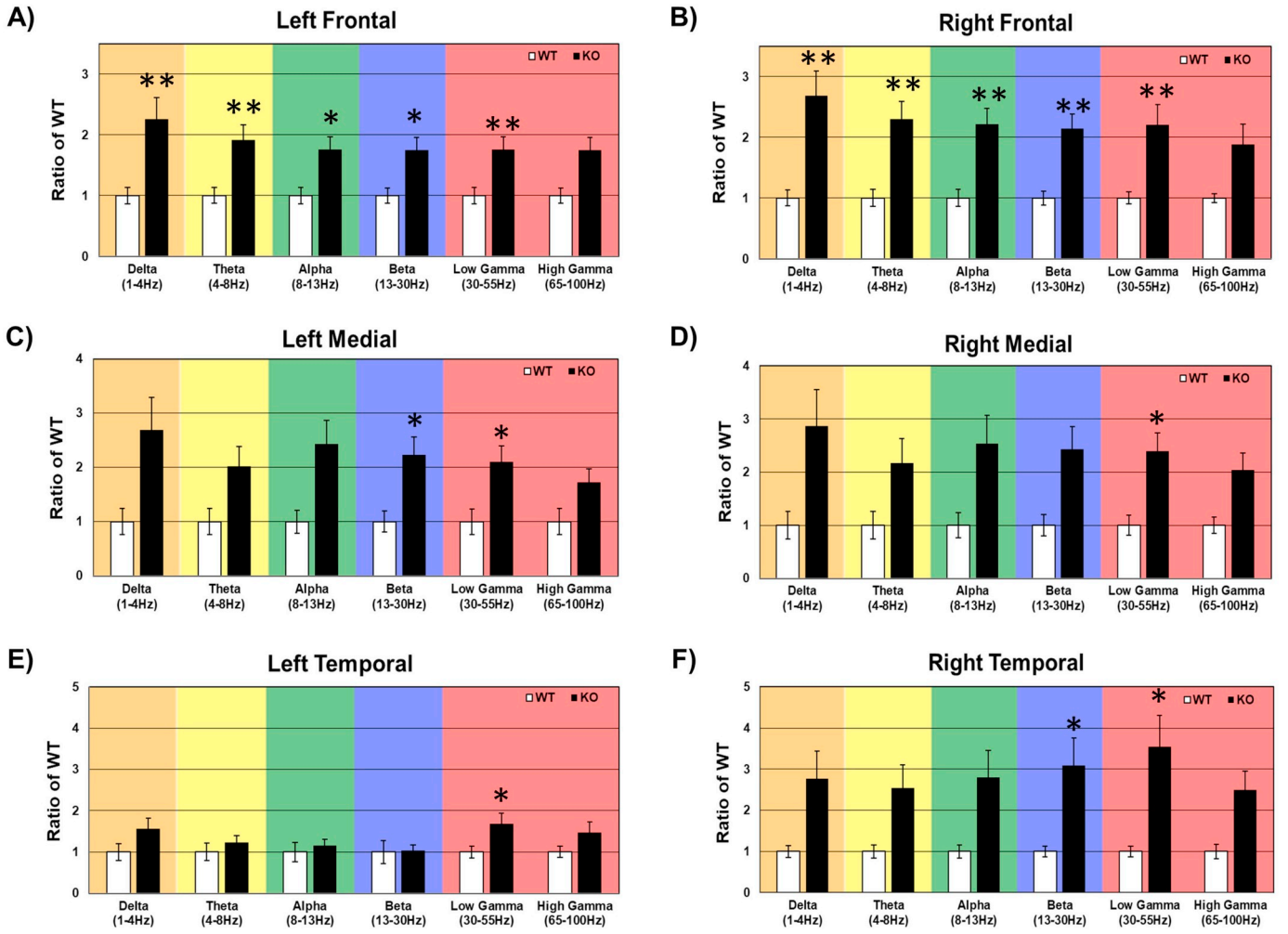

Fig. 4. Quantitation of ratio of *Fmr1* KO to WT EEG power across frequency bands for distinct brain regions **(A–F)**. Values above 1 indicate higher EEG power in *Fmr1* KO compared with WT mice. $*p < .05$; $**p < .01$. $n = 11$ *Fmr1* KO, $n = 10$ WT mice.

2.6. Statistical analyses

The term 'resting' is used to indicate EEGs recorded in these mice without any specific auditory stimuli. The data were analyzed for 2 factors: Genotype (WT, *Fmr1* KO) and Frequency (delta to gamma) for the cortical regions (left frontal, right frontal, left medial, right medial, left temporal and right temporal). We analyzed the raw data using 2-way ANOVA. Data were expressed as ratio of WT values to gauge relative differences in various factors using the same scale.

Statistical group comparisons of broadband noise trains and chirp responses (ITPC) were quantified by wavelet analysis. Statistical analysis was conducted by binning time into 625 parts and frequency into 100 parts, resulting in a 100 × 625 matrix. Non-parametric cluster analysis was used to determine contiguous regions in the matrix that were significantly different from a distribution of 1000 randomized Monte Carlo permutations based on previously published methods (Maris and Oostenveld, 2007). Briefly, if the cluster sizes of the real genotype assignments (both positive and negative direction, resulting in a two-tailed alpha of $p = .025$) were larger than 97.25% of the random group assignments, those clusters were considered significantly different between genotypes. This method avoids statistical assumptions about the data and corrects for multiple comparisons.

In all cases where genotype means are reported, SEM was used. In all cases, p values $< .05$ were considered significant for ANOVA and Student's *t*-tests. Where t-tests were performed, r was calculated as an effect size. When interactions were found and multiple comparisons for ANOVA were made, data were analyzed on each factor for simple effects and corrected for using Bonferroni adjustments. If assumptions of sphericity were violated for repeated measures ANOVA, the Greenhouse-Geiser correction was used.

3. Results

3.1. Multielectrode array analysis of resting EEG

We developed a method for stable chronic *in vivo* implantation of a planar MEA on the surface of the mouse skull (Fig. 1) (Jonak et al., 2018). This can then be used for baseline and stimulus-evoked EEG acquisition in awake, freely moving mice. Features of our protocol include: (1) standardized implantation procedure; (2) reproducible placement of probe over the skull surface with bregma as reference; (3) Teflon/plastic wrap protective layer for the MEA probe to enable reusability; (4) secure implantation with dental cement and screw fixation; (5) fixation of the headstage with an anchoring "post"; (6) use of commutator to allow free movement of the mouse and cables without restriction; (7) reproducible artifact-free 30-channel EEG; and (8) reusability of the MEA probes. With this method, we reliably obtain 30-channel low-noise EEG from awake mice. Resting and stimulus-evoked EEG recordings can be readily obtained and analyzed. In the current study, we applied this MEA technology to analyze resting and stimulus-evoked EEG in the Fragile X mouse model, *Fmr1* KO mice. An example of resting 30-channel MEA EEG obtained from WT *vs.* *Fmr1* KO mice is

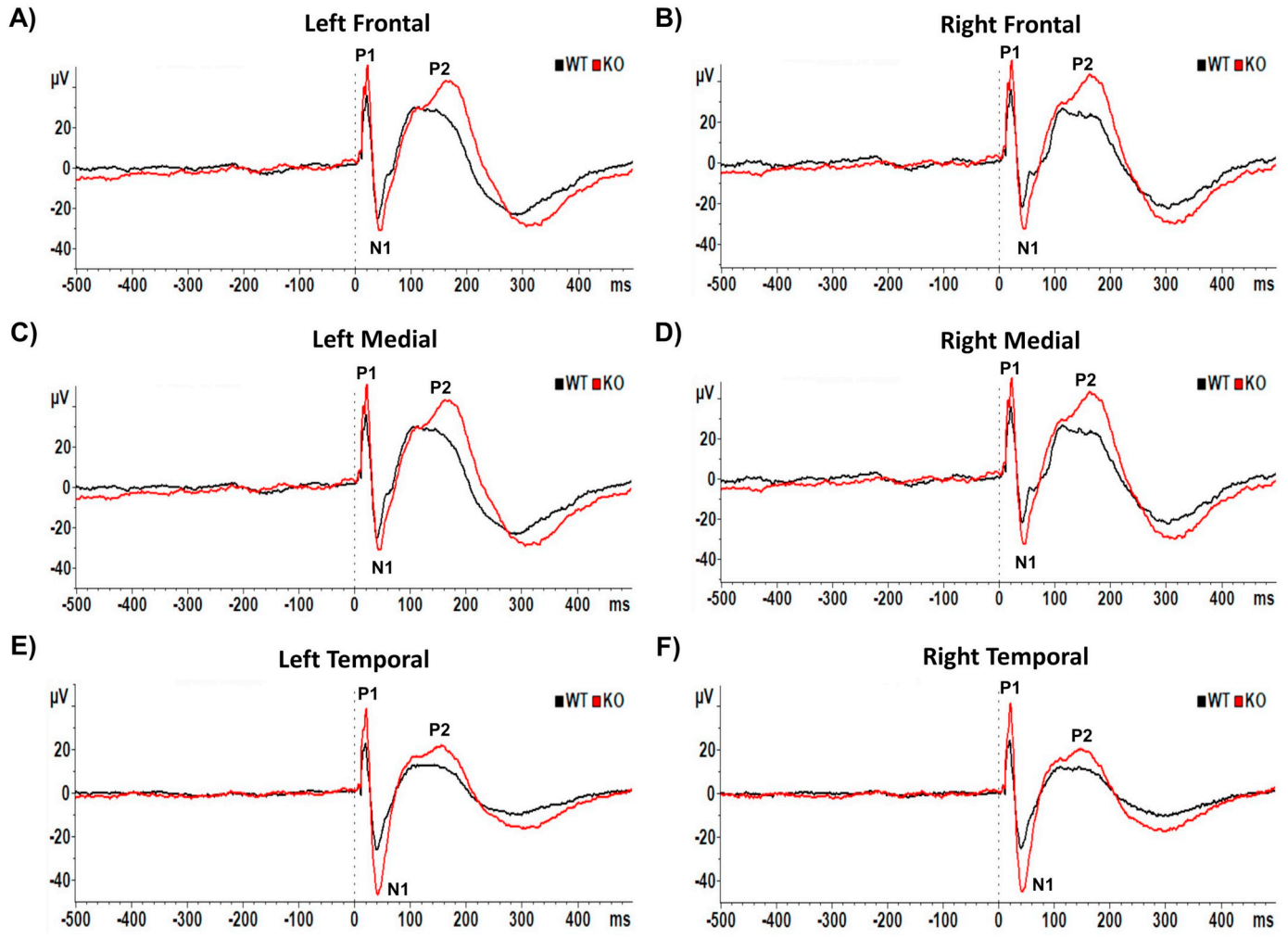

Fig. 5. Multielectrode array analysis of auditory event-related potentials (ERPs) in WT *vs. Fmr1* KO mice. Single ERP peak analysis was done by obtaining average traces across the first response of all BBN trains (total of 200 trials). Peaks were determined by pre-defined time windows after stimulus onset: P1 (10–30 ms), N1 (30–75 ms), and P2 (75–150 ms). WT and *Fmr1* KO ERP morphologies are shown by brain region.

shown in Fig. 2. This demonstrates that low-noise resting MEA EEG can be obtained, and qualitative visual comparison suggests a difference in amplitude and frequency characteristics of the resting EEG between WT and *Fmr1* KO mice. To further evaluate spectral characteristics of baseline MEA EEG in WT *vs. Fmr1* KO mice, we performed power spectral density analysis across brain regions (left frontal, right frontal, left medial, right medial, left temporal, right temporal). These six regions (Fig. 1B) were empirically defined electrode clusters by region to allow group comparisons, although of course any combination of the 30 electrodes could be used or compared if desired. *Fmr1* KO mice were found to have higher resting EEG power across frequency bands (Fig. 3). Interestingly, there was a trend toward higher resting EEG power in the right hemisphere compared with the left hemisphere in *Fmr1* KO mice, especially in the temporal region (Fig. 3F *vs.* Fig. 3E).

Resting EEG data were then analyzed with two-way ANOVA for 2 factors: Genotype (WT, *Fmr1* KO) and Frequency (delta to gamma) for the cortical regions (left frontal, right frontal, left medial, right medial, left temporal and right temporal) (Fig. 4). In the left frontal region, significant increases in EEG power in *Fmr1* KO mice were found in delta, theta, alpha, beta, and low gamma frequency bands (Fig. 4A). In the right frontal region, increases in delta, theta, alpha, beta, and low gamma power were found as well (Fig. 4B). In the left medial region, significant increases in EEG power in *Fmr1* KO mice were found in beta and low gamma bands (Fig. 4C). In the right medial region, a significant increase was found just in low gamma power (Fig. 4D). In the left temporal region, a significant increase was found just in low gamma power (Fig. 4E). In the right temporal region, significant increases in beta and low gamma power was observed (Fig. 4F). These data are based on MEA analyses of $n = 11$ *Fmr1* KO and $n = 10$ WT mice. These data show significant increases in EEG power in distinct frequency bands and different cortical areas in awake and freely moving *Fmr1* KO mice compared to WT mice.

3.2. Increased amplitude of auditory ERPs in Fmr1 KO mice

Next, we aimed to detect and analyze auditory event-related potentials (ERPs) using our *in vivo* MEA system. Indeed, we were able to record auditory ERPs from 1 Hz broadband noise with normal morphologies, as well as identify and quantify P1, N1, and P2 components (Fig. 5). We subsequently analyzed ERP component amplitudes and latencies by brain region in the same WT and *Fmr1* KO mice that were subjected to resting EEG analysis (n = 11 *Fmr1* KO, n = 10 WT). In *Fmr1* KO mice, significant increases were found in left frontal P1 amplitude (Fig. 6A), left frontal P2 latency (Fig. 6B), left and right medial N1 amplitudes (Fig. 6C), left temporal P1, N1, and P2 amplitudes and right temporal N1 and P2 amplitudes (Fig. 6E). Therefore, we did find increased ERP N1 amplitudes described previously in other studies (Lovelace et al., 2018) but interestingly these were region-specific, with significantly increased N1 amplitudes in the medial and temporal regions, but not the frontal region.

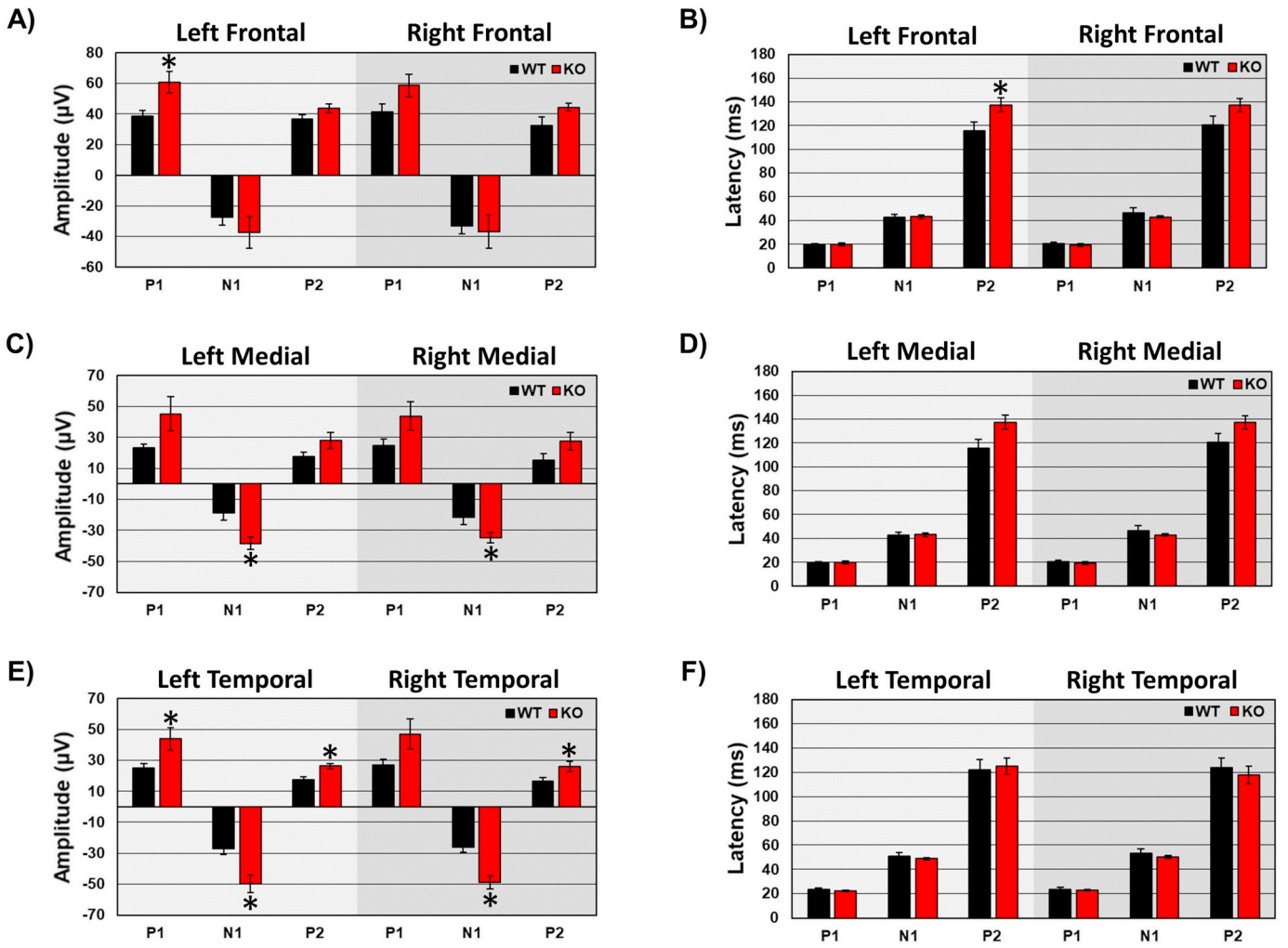

Fig. 6. Quantitation of auditory event-related potential (ERP) amplitudes and latencies in WT *vs. Fmr1* KO mice. In *Fmr1* KO mice, significant increases were found in left frontal P1 amplitude (A), left frontal P2 latency (B), left and right medial N1 amplitudes (C), left temporal P1, N1, and P2 amplitudes and right temporal N1 and P2 amplitudes (E). $^{*}p < .05$. n = 11 *Fmr1* KO, n = 10 WT mice.

3.3. Increased event-related power following auditory stimulation in Fmr1 KO mice

Previous studies found increases in event-related power in *Fmr1* KO mice following auditory stimulation (Lovelace et al., 2019), but potential region-specific differences are not known. Therefore, we analyzed event-related power from the MEA data following auditory stimulation (both single and train stimulation). Event-related power following the first auditory stimulation of each train revealed significant differences between WT and *Fmr1* KO mice. *Fmr1* KO mice demonstrated increased event-related power in all brain regions (Fig. 7A, C, D, E, F) except right frontal (Fig. 7B), indicating that the increased power following a sound stimulus is essentially a brain-wide phenomenon providing important insight into neural correlates of sensory hypersensitivity.

We also analyzed event-related power during entire 1 Hz trains of BBN auditory stimuli. Each BBN stimulus in the train led to a measurable stimulus-related EEG power response (Fig. 8). Significant differences in 1 Hz train event-related power were noted between WT and *Fmr1* KO mice. *Fmr1* KO mice demonstrated increased 1 Hz train event-related power in all brain regions (Fig. 8A–F).

3.4. Reduced phase locking in Fmr1 KO mice to temporally modulated stimuli

Inter-trial phase coherence (ITPC) (also called phase locking factor) measures the reliability of synchronization of neural responses to repetitions of the auditory chirp stimuli, with the EEG response entrained to the chirp modulation frequency (Fig. 9). In WT mice, there was a robust response to the chirp stimulus throughout the brain regions studied (Fig. 9A–F, left panels). In *Fmr1* KO mice, ITPC following chirp stimulation was significantly decreased in all brain regions (Fig. 9A–F, middle and right panels). In particular, ITPC in *Fmr1* KO mice appeared to be decreased in a specific frequency band ranging from approximately 40–60 Hz (low gamma range) (Fig. 9A–F, right panels). Thus, there was a marked deficit in phase locking to the frequency modulated auditory stimulus in *Fmr1* KO mice throughout the brain, particularly in the low gamma range.

4. Discussion

In this paper, we used 30-channel mouse skull surface MEA in *Fmr1* KO mice *vs.* WT mice for the first time and generated several novel findings. First, *Fmr1* KO mice were found to have higher resting EEG power across multiple frequency bands. Second, the specific frequency bands (delta, theta, alpha, beta, and low gamma) that demonstrated

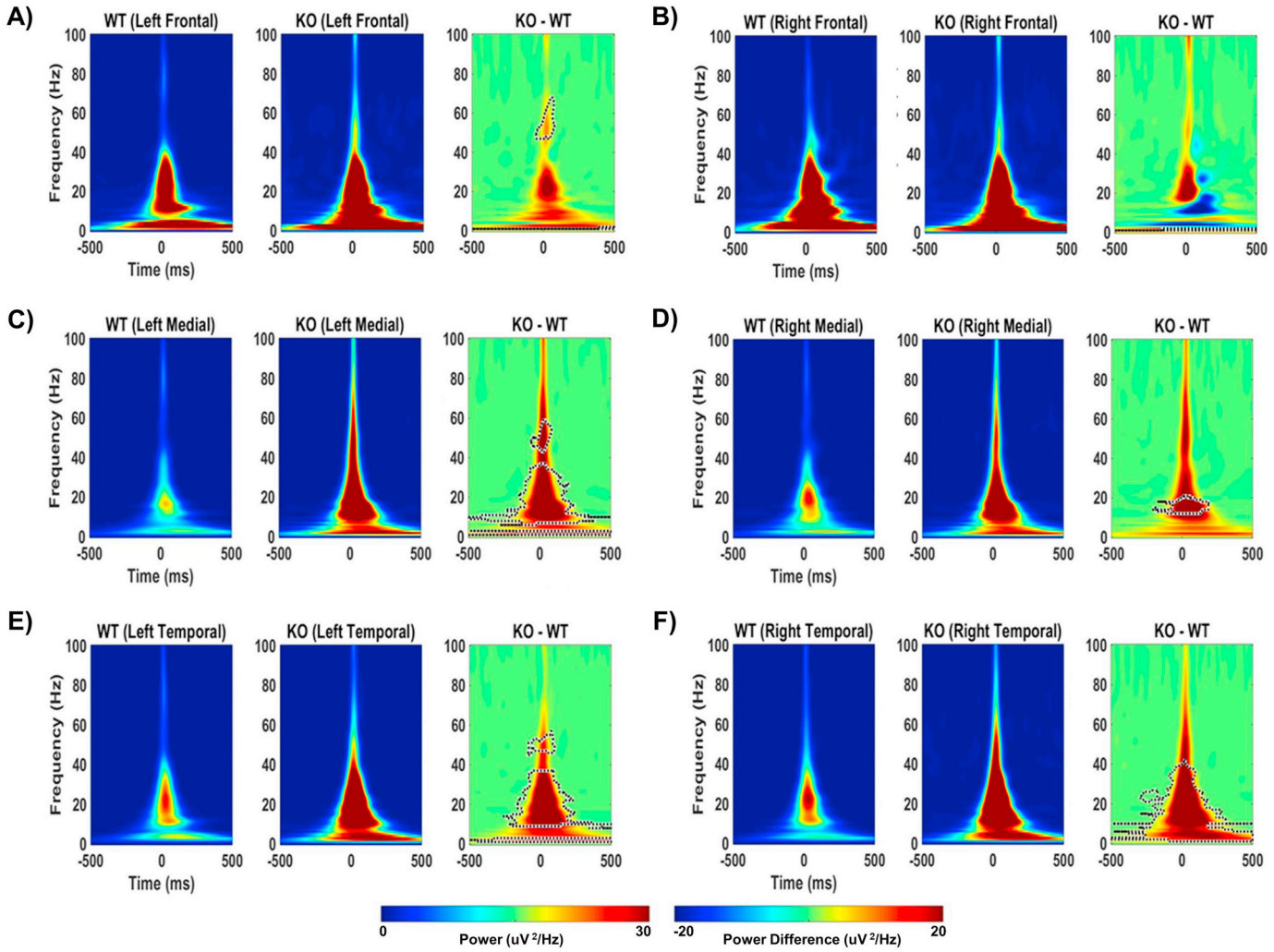

Fig. 7. Single-trial event-related power following auditory stimulation in WT *vs. Fmr1* KO mice. For each brain region (A-F), the left panel shows the averaged WT event-related power, the middle panel shows the averaged *Fmr1* KO event-related power and the right panel shows KO-WT (subtraction). Scales at the bottom show power and power difference in μV^2/Hz. Significant increases in event-related power in *Fmr1* KO compared to WT mice are outlined in black-dotted areas.

increased resting EEG power in *Fmr1* KO mice were region-specific. Third, significant region-specific alterations in ERP component amplitudes were observed in *Fmr1* KO mice. Fourth, *Fmr1* KO mice demonstrated increased sound-induced power in all brain regions. Fifth, inter-trial phase coherence to auditory "chirp" stimuli was significantly decreased in all brain regions in *Fmr1* KO mice. These findings provide a robust set of EEG phenotypes that are likely neural correlates of sensory hypersensitivity in FXS, and indicate remarkably similar EEG phenotypes in *Fmr1* KO mice and humans with FXS.

4.1. Genotype differences in resting EEG power spectral density

Our previous studies demonstrated increased resting state gamma (30–100 Hz) power in auditory and frontal cortex of *Fmr1* KO mice (Lovelace et al., 2018, 2019). Enhanced resting gamma power is consistent with a previous study of *Fmr1* KO mice (Sinclair et al., 2017a). Our current findings demonstrate widespread increases in resting EEG power across multiple frequency bands in *Fmr1* KO mice (Fig. 3). This indicates that the increase in resting EEG power is a global brain-wide phenomenon in *Fmr1* KO mice. Interestingly, changes in EEG power were not limited to the gamma frequency. It is possible that the 30-channel MEA provides much greater sensitivity to the EEG changes at lower frequencies than prior studies (Lovelace et al., 2018; Sinclair et al., 2017a). In the frontal region, for example, increases in EEG power in *Fmr1* KO mice were observed in delta, theta, alpha, beta, and low gamma bands (Fig. 4A, B). Furthermore, these increases were region-specific, with medial and temporal regions exhibiting significant increases in low gamma (Fig. 4E, F). In addition, increases in EEG power in *Fmr1* KO mice appeared more pronounced in right temporal *vs.* left temporal regions (Fig. 3F *vs.* Fig. 3E). In this initial report with the MEA technique, we elected to group 30-channel data into these 6 "regions" to make these comparisons, but clearly it is feasible to individually analyze each of the 30 single channels if desired, other anatomic groupings and/or hemispheric lateralization (Fig. 1B). Future studies will also be able to test whether these resting EEG changes are normalized with pharmacological treatment.

4.2. Genotype differences in ERPs and event-related power

Studies of humans with FXS have demonstrated alterations in ERPs including increased N1 amplitude (Castrén et al., 2003; Van der Molen et al., 2012). Our previous 2-channel study in the *Fmr1* KO mice demonstrated increased N1 amplitude and increased event-related power (Wen et al., 2019). Interestingly, in the current MEA study we found significantly increased N1 amplitudes in the medial and temporal regions bilaterally but not the frontal region (Figs. 5 and 6). ERP latencies were not found to be different except for left frontal P2 (Fig. 6B). In contrast, event-related power was significantly higher in *all* brain

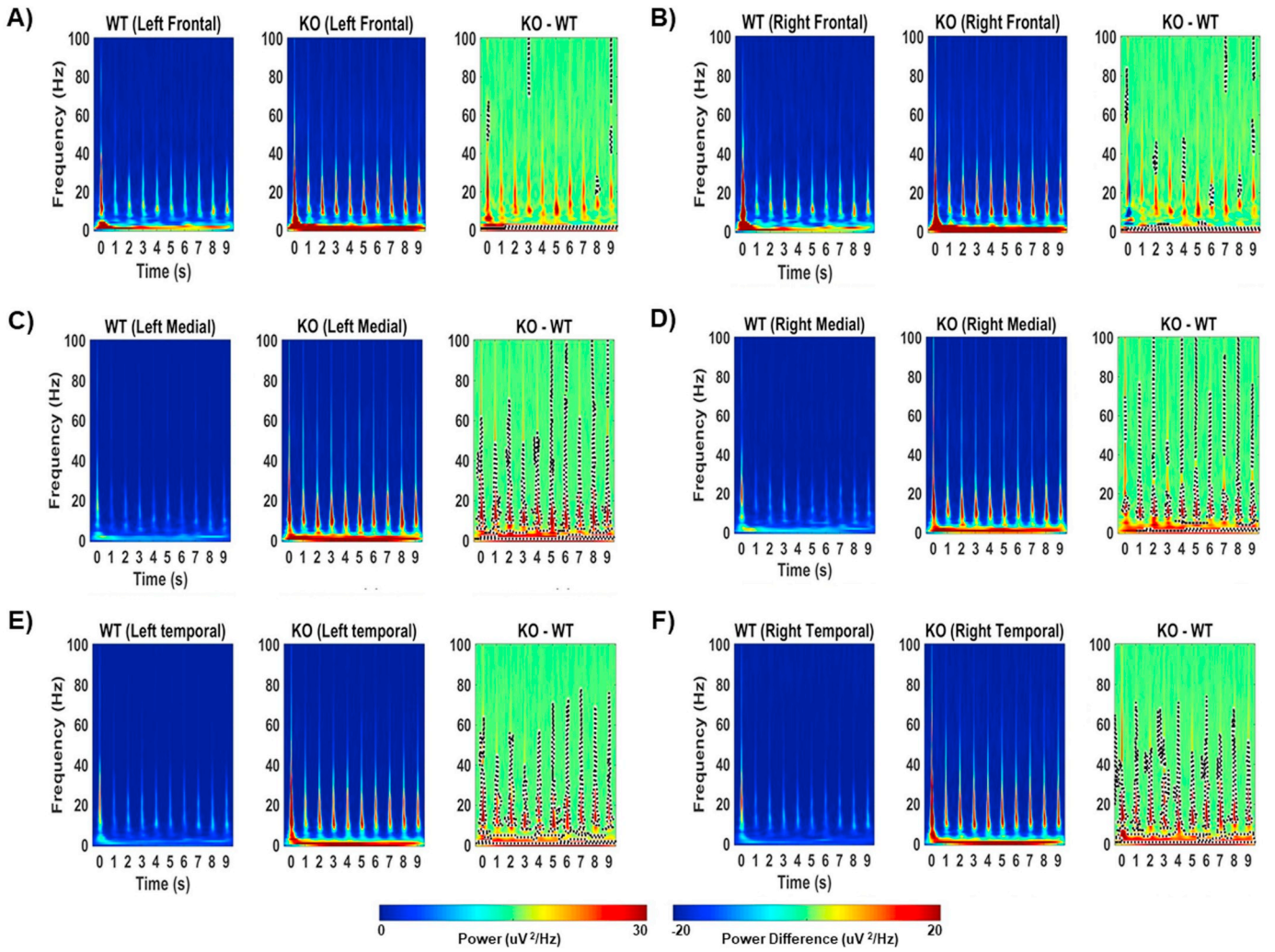

Fig. 8. Event-related power following 1 Hz train of auditory stimulation in WT *vs. Fmr1* KO mice. For each brain region (A–F), the left panel shows the averaged WT event-related power, the middle panel shows the averaged *Fmr1* KO event-related power and the right panel shows KO-WT. Scales at the bottom show power and power difference in μV^2/Hz. Significant increases in event-related power in *Fmr1* KO compared to WT mice are outlined in black-dotted areas.

regions except right frontal when assessed as single-trial power (Fig. 7) and in *all* brain regions in response to 1 Hz stimulus trains (Fig. 8). Thus, event-related power (either single stimulus or train) may be a more reliable EEG biomarker than ERP amplitudes and latencies to distinguish WT and *Fmr1* KO mice. Furthermore, we note that event-related power data are not dependent on ERP morphology characteristics but rather show the overall "power" response of the brain to the auditory stimulus. As such, frequency characteristics can also be distinguished which provide more information than ERP amplitude and latency.

Enhancement of ERP N1 amplitude and event-related power is likely to be related to underlying neurophysiological response magnitudes to a given auditory stimulus. Previous studies in the adult *Fmr1* KO mice auditory cortex showed enhanced responses to tones and broader frequency tuning of single neurons (Rotschafer and Razak, 2013). In addition, there is reduced habituation of ERPs to repeated sounds in *Fmr1* KO mice as compared to WT mice (Lovelace et al., 2016). Together, these data indicate that for any sound, more neurons will respond with a greater response magnitude over a sustained period. The observations of enhanced ERP amplitude as well as single-trial and 1 Hz train-related power are consistent with this interpretation. Overall, these and our previous results (Lovelace et al., 2018, 2019) in auditory cortex are similar to other findings of sensory hyperexcitability due to circuit changes in *Fmr1* KO mice. For example, there is an abnormally large size of whisker-evoked somatosensory cortical maps in adult *Fmr1* KO mice (He et al., 2019). Various circuit alterations including single cell response magnitudes, developmental changes involving inhibitory circuitry and overall circuit synchrony may account for these changes (Berzhanskaya et al., 2017; Contractor et al., 2015; Goncalves et al., 2013; Sinclair et al., 2017b; Talbot et al., 2018; Wen et al., 2018).

4.3. Genotype differences in evoked neural synchronization

Recent EEG studies of humans with FXS have reported enhanced resting gamma power, reduced chirp-evoked phase locking in gamma frequencies and enhanced single-trial power (Ethridge et al., 2017; Wang et al., 2017). These EEG abnormalities were correlated with clinically relevant measures including heightened sensory sensitivity and autism-associated social impairment (Social Communication Questionnaire), indicating translational relevance (Ethridge et al., 2017). Given the robust recent human data indicating reduced chirp-evoked phase locking in gamma frequencies, we aimed to determine whether this could be reliably observed in the *Fmr1* KO mice with MEA analysis. Indeed, we observed a marked impairment in ITPC or "phase-locking" to chirp stimuli in *Fmr1* KO mice (Fig. 9) indicating reduced ability to synchronize to the frequency-modulated stimulus. ITPC following auditory chirp stimulation was significantly decreased in *all* brain regions. Interestingly, this appeared to be frequency-specific, with

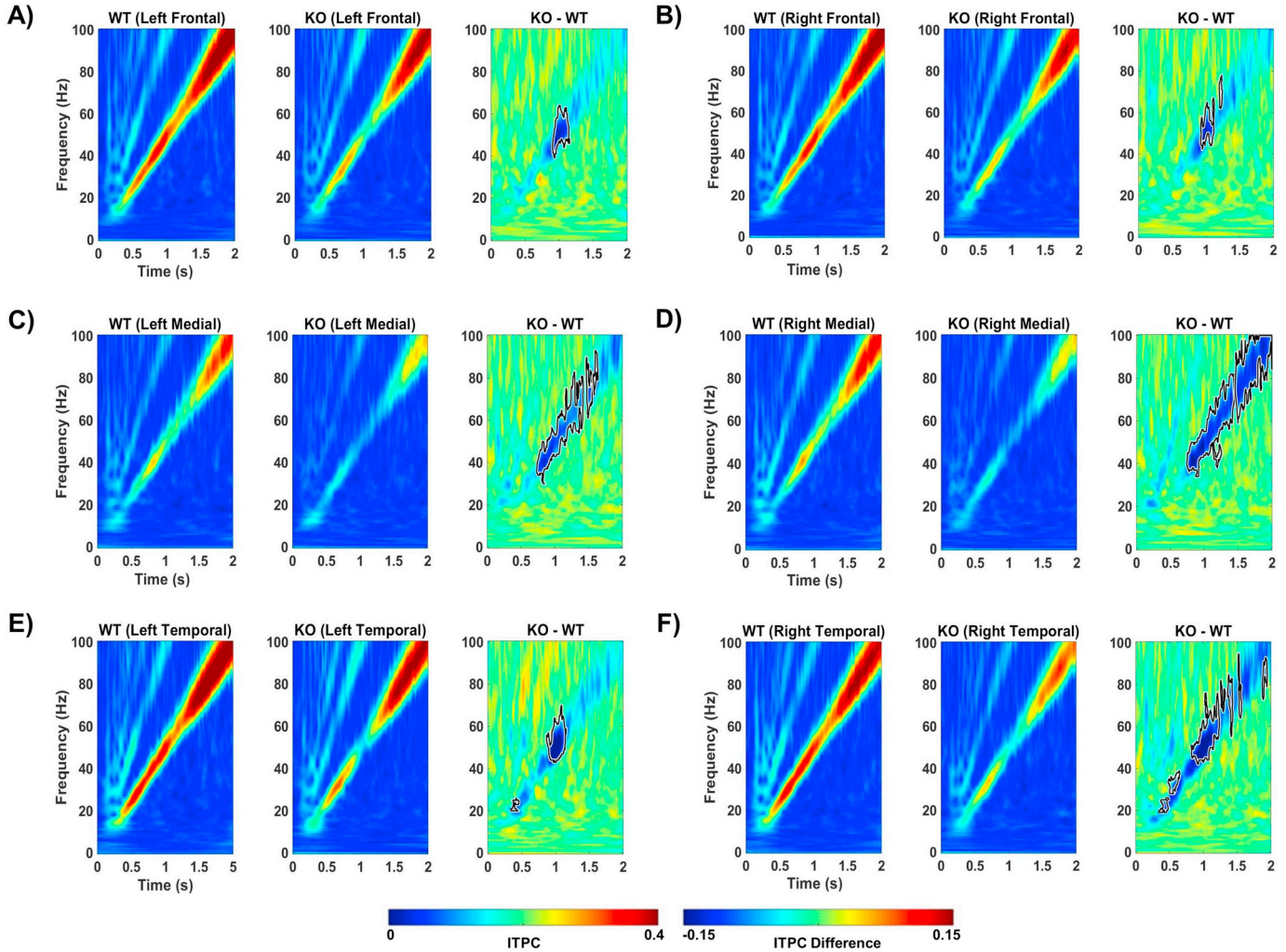

Fig. 9. Multielectrode array analysis of auditory chirp stimulation in WT *vs. Fmr1* KO mice. For each brain region (A–F), the left panel shows the averaged WT inter-trial phase coherence (ITPC or phase-locking factor), the middle panel shows the averaged *Fmr1* KO ITPC and the right panel shows KO-WT. Scales at the bottom show ITPC and ITPC difference in μV^2/Hz. Significant decreases in ITPC in *Fmr1* KO compared to WT mice are shown in black-outlined areas. Blue areas in the right panels (KO-WT) are negative ITPC differences since ITPC values in KO are less than WT mice. (For interpretation of the references to colour in this figure legend, the reader is referred to the web version of this article.)

the greatest deficit in phase locking in the 40–60 Hz range (Fig. 9). Thus, ITPC following auditory chirp stimulation may be a reliable EEG biomarker to distinguish stimulus-induced brain responses in WT *vs. Fmr1* KO mice and in human studies (Ethridge et al., 2017).

4.4. Parallel EEG abnormalities in Fmr1 KO mice and FXS humans

Several parallel EEG abnormalities have been observed in both humans with FXS and *Fmr1* KO mice: (1) enhanced resting gamma power; (2) enhanced single-trial power; and (3) reduced phase-locking to chirp stimuli. We hypothesize that this combination of factors may be associated with both sensory hypersensitivity and also reduced auditory stimulus discrimination more generally. Previous studies have found deficits in auditory information processing in FXS patients, such as impaired auditory stimulus discrimination (Van der Molen et al., 2012). Our model would predict that enhanced resting gamma (in the un-stimulated brain) constitutes background "gamma noise" that would impair synchronized response to a stimulus, particularly in the gamma range. Hence, the ITPC deficit appears particularly in the low gamma range, where we observed significant increase in resting EEG power. Increased single-trial power, which we also observe in parallel with the human data, may relate to auditory cortical hyperexcitability; however, an exaggerated cortical response to individual stimuli together with background "gamma noise" would presumably be maladaptive in generating temporally synchronized responses to rapid auditory stimuli. This hypothesis could be tested by determining whether pharmacological interventions that ameliorate the above EEG abnormalities also improve auditory stimulus discrimination. Proof-of-principle for this comes from a study in which racemic baclofen, a $GABA_B$ agonist, was able to improve working memory and anxiety-related behavior in conjunction with reduction in auditory-evoked gamma oscillations (Sinclair et al., 2017a). Alternatively, selective manipulation of inhibition could be employed as has been done recently to restore parvalbumin neuron function in *Fmr1* KO mouse visual cortex resulting in improvement in visual discrimination (Goel et al., 2018).

The similarity in EEG measures between humans and mice indicate that EEG/ERP recordings can serve as objective, physiological probes that serve as surrogate biomarkers to develop therapeutics to treat symptoms of FXS (Schneider et al., 2013; Sinclair et al., 2017a). More broadly, increased high-frequency EEG power has been found in autism spectrum disorders (Orekhova et al., 2007; Sinclair et al., 2017b; Wang et al., 2013). Low-frequency EEG abnormalities have also been found in humans with FXS with enhanced theta band power relative to healthy controls (Van der Molen and Van der Molen, 2013b; Wang et al., 2017).

These similarities in EEG measures between humans and mice suggest the importance of studying basic sensory processing using analogous experimental design and approach in generating translation-relevant biomarkers (Sinclair et al., 2017b). These measures may be useful outcome measures in the preclinical to clinical drug development pipeline and can be also employed in stratification of patient population for appropriate treatment strategies using a combination of EEGs and pharmacology. In particular, the finding that a particular drug candidate has robust effects on normalizing EEG parameters such as resting gamma power and phase-locked synchronization in both humans and mice would enable targeting and correlation of those drugs with clinical parameters (Berry-Kravis et al., 2018).

We envision MEA EEG analysis in particular to be useful in several distinct contexts in mouse models of neurodevelopmental disorders (NDD) (Ewen et al., 2019; Vasa et al., 2016). (1) *Further delineation of EEG biomarkers*. Simply having 30 channels to compare as opposed to 2 channels in our previous studies has enabled more region-specific analysis. Distinct stimulus parameters could also be used with the same MEA system, such as visual evoked potentials (VEPs) (Land et al., 2019). Furthermore, more complex EEG parameters can be derived from the 30-channel MEA data. In addition to resting EEG power, ERP amplitudes and latencies, single-trial power and ITPC as reported in this study, the availability of 30 channels with a well-defined spatial orientation (Fig. 1) enables spatial analysis of EEG signal propagation across the cortical surface as well as analysis of phase synchronization (Jonak et al., 2018; Wang et al., 2013), cross-frequency amplitude coupling, and phase-amplitude coupling (Munia and Aviyente, 2019). Altered theta-gamma coupling and increased phase synchronization were observed in FXS subjects (Wang et al., 2017), parameters which can now be derived with mouse MEA analysis. Altered cross-frequency coupling has been correlated to cognition in several other contexts (Munia and Aviyente, 2019; Rodriguez-Larios and Alaerts, 2019) and is feasible with high-density mouse MEA data. Derivation of such measures in *Fmr1* KO mice or other animal models of FXS (Dahlhaus, 2018) may uncover additional EEG biomarkers specific to FXS pathophysiology. In addition, application of MEA to other models of NDD may similarly enable identification of translational EEG biomarkers. For example, in Rett syndrome (RTT), specific changes in EEG spectral power have been correlated with lower cognitive assessment scores (Roche et al., 2019); thus, use of MEA EEG in animal models of RTT may enable identification of parallel MEA EEG biomarkers in RTT animal models, enabling use as therapeutic targets. Another example is Angelman syndrome, in which delta rhythmicity (Sidorov et al., 2017) and gamma coherence during sleep (den Bakker et al., 2018) have been associated with the disease state. (2) *Pharmacological studies*. We have demonstrated feasibility in affixing the 30-channel MEA to the skull surface of awake, behaving mice for several weeks (Jonak et al., 2018) allowing both acute and chronic studies of drug effects on EEG parameters/biomarkers in *Fmr1* KO mice (or for any other mouse model). Each candidate drug could then be assessed for its efficacy in normalizing MEA EEG parameters with both acute and chronic administration. (3) *Mechanistic studies*. Combined use of the MEA EEG system with genetic mouse models and/or DREADDs could enable dissection of cell type-specific contributions to EEG abnormalities in FXS and in NDD more generally. For example, selective deletion of *Fmr1* from forebrain excitatory neurons has recently been found to increase resting EEG gamma power (Lovelace et al., 2019); MEA analysis with parameters described above could assess the effects of multiple distinct cell-type-specific deletions on specific MEA EEG parameters.

In summary, we have employed MEA EEG analysis in *Fmr1* KO *vs.* WT mice for the first time. These studies have revealed specific EEG biomarkers in this FXS mouse model. We believe that the MEA system will serve as a robust method for further definition of EEG biomarkers in diverse disorders as well as an enabling technology for mechanistic and therapeutic studies.

Declaration of Competing Interest

None.

Acknowledgements

We thank members of the Ethell, Razak, and Binder laboratories for helpful discussions. This work was supported by the National Institutes of Health (NIH) (1U54 HD082008-01 to IME, KAR and DKB) and US Army Medical Research (W81XWH-15-1-0436 to IME, KAR and DKB).

References

Abbeduto, L., Hagerman, R.J., 1997. Language and communication in Fragile X syndrome. Ment. Retard. Dev. Disabil. Res. Rev. 3, 313–322.
Artieda, J., et al., 2004. Potentials evoked by chirp-modulated tones: a new technique to evaluate oscillatory activity in the auditory pathway. Clin. Neurophysiol. 115, 699–709.
Bakker, C.E., et al., 1994. Fmr1 knockout mice: a model to study Fragile X mental retardation. The Dutch-Belgian Fragile X Consortium. Cell. 78, 23–33.
den Bakker, H., et al., 2018. Abnormal coherence and sleep composition in children with Angelman syndrome: a retrospective EEG study. Mol. Autism. 9, 32.
Bernardet, M., Crusio, W.E., 2006. Fmr1 KO mice as a possible model of autistic features. TheScientificWorldJournal. 6, 1164–1176.
Berry-Kravis, E., 2002. Epilepsy in Fragile X syndrome. Dev. Med. Child Neurol. 44, 724–728.
Berry-Kravis, E.M., et al., 2018. Drug development for neurodevelopmental disorders: lessons learned from Fragile X syndrome. Nat. Rev. Drug Discov. 17, 280–299.
Berzhanskaya, J., et al., 2017. Disrupted cortical state regulation in a rat model of Fragile X syndrome. Cereb. Cortex 27, 1386–1400.
Castrén, M., et al., 2003. Augmentation of auditory N1 in children with Fragile X syndrome. Brain Topogr. 15, 165–171.
Contractor, A., et al., 2015. Altered neuronal and circuit excitability in Fragile X syndrome. Neuron. 87, 699–715.
Crawford, D.C., et al., 2001. FMR1 and the Fragile X syndrome: human genome epidemiology review. Genet. Med. 3, 359–371.
Dahlhaus, R., 2018. Of men and mice: modeling the fragile X syndrome. Front. Mol. Neurosci. 11, 41.
Darnell, J.C., et al., 2011. FMRP stalls ribosomal translocation on mRNAs linked to synaptic function and autism. Cell. 146, 247–261.
Ethridge, L.E., et al., 2016. Reduced habituation of auditory evoked potentials indicate cortical hyper-excitability in Fragile X syndrome. Transl. Psychiatry 6, e787.
Ethridge, L.E., et al., 2017. Neural synchronization deficits linked to cortical hyper-excitability and auditory hypersensitivity in fragile X syndrome. Mol. Autism. 8, 22.
Ewen, J.B., et al., 2019. Conceptual, regulatory and strategic imperatives in the early days of EEG-based biomarker validation for neurodevelopmental disabilities. Front. Integr. Neurosci. 13, 45.
Goel, A., et al., 2018. Impaired perceptual learning in a mouse model of Fragile X syndrome is mediated by parvalbumin neuron dysfunction and is reversible. Nat. Neurosci. 21, 1404–1411.
Goncalves, J.T., et al., 2013. Circuit level defects in the developing neocortex of fragile X mice. Nat. Neurosci. 16, 903–909.
Hagerman, R.J., et al., 2009. Advances in the treatment of fragile X syndrome. Pediatrics. 123, 378–390.
He, Q., et al., 2019. Critical period inhibition of NKCC1 rectifies synapse plasticity in the somatosensory cortex and restores adult tactile response maps in fragile X mice. Mol. Psychiatry 24, 1732–1747.
Jonak, C.R., et al., 2018. Reusable multielectrode array technique for electroencephalography in awake freely moving mice. Front. Integr. Neurosci. 12, 53.
Land, R., et al., 2019. 32-channel mouse EEG: visual evoked potentials. J. Neurosci. Methods 325, 108316.
Lovelace, J.W., et al., 2016. Matrix metalloproteinase-9 deletion rescues auditory evoked potential habituation deficit in a mouse model of Fragile X syndrome. Neurobiol. Dis. 89, 126–135.
Lovelace, J.W., et al., 2018. Translation-relevant EEG phenotypes in a mouse model of fragile X syndrome. Neurobiol. Dis. 115, 39–48.
Lovelace, J.W., et al., 2019. Deletion of Fmr1 from forebrain excitatory neurons triggers abnormal cellular, EEG, and behavioral phenotypes in the auditory cortex of a mouse model of Fragile X syndrome. Cereb. Cortex. https://doi.org/10.1093/cercor/bhz141. pii: bhz141, (Epub ahead of print).
Maris, E., Oostenveld, R., 2007. Nonparametric statistical testing of EEG- and MEG-data. J. Neurosci. Methods 164, 177–190.
Miller, L.J., et al., 1999. Electrodermal responses to sensory stimuli in individuals with fragile X syndrome: a preliminary report. Am. J. Med. Genet. 83, 268–279.
Munia, T.T.K., Aviyente, S., 2019. Time-frequency based phase-amplitude coupling measure for neuronal oscillations. Sci. Rep. 9, 12441.
Musumeci, S.A., et al., 1999. Epilepsy and EEG findings in males with Fragile X syndrome. Epilepsia. 40, 1092–1099.
Orekhova, E.V., et al., 2007. Excess of high frequency electroencephalogram oscillations in boys with autism. Biol. Psychiatry 62, 1022–1029.
Pérez-Alcázar, M., et al., 2008. Chirp-evoked potentials in the awake and anesthetized rat. A procedure to assess changes in cortical oscillatory activity. Exp. Neurol. 210,

144–153.
Purcell, D.W., et al., 2004. Human temporal auditory acuity as assessed by envelope following responses. J. Acoust. Soc. Am. 116, 3581–3593.
Roberts, J.E., et al., 2001. Development and behavior of male toddlers with Fragile X syndrome. J. Early Interv. 24, 207–223.
Roche, K.J., et al., 2019. Electroencephalographic spectral power as a marker of cortical function and disease severity in girls with Rett syndrome. J. Neurodev. Disord. 11, 15.
Rodriguez-Larios, J., Alaerts, K., 2019. Tracking transient changes in the neural frequency architecture: harmonic relationships between theta and alpha peaks facilitate cognitive performance. J. Neurosci. 39, 6291–6298.
Rotschafer, S., Razak, K., 2013. Altered auditory processing in a mouse model of Fragile X syndrome. Brain Res. 1506, 12–24.
Rotschafer, S.E., Razak, K.A., 2014. Auditory processing in Fragile X syndrome. Front. Cell. Neurosci. 8, 19.
Sabaratnam, M., et al., 2001. Epilepsy and EEG findings in 18 males with Fragile X syndrome. Seizure. 10, 60–63.
Schneider, A., et al., 2013. Electrocortical changes associated with minocycline treatment in Fragile X syndrome. J. Psychopharmacol. 27, 956–963.
Sidorov, M.S., et al., 2017. Delta rhythmicity is a reliable EEG biomarker in Angelman syndrome: a parallel mouse and human analysis. J. Neurodev. Disord. 9, 17.
Sinclair, D., et al., 2017a. GABA-B agonist baclofen normalizes auditory-evoked neural oscillations and behavioral deficits in the < i > Fmr1 < /i > knockout mouse model of Fragile X syndrome. ENEURO 4 (ENEURO.0380-16.2017).
Sinclair, D., et al., 2017b. Sensory processing in autism spectrum disorders and fragile X syndrome-from the clinic to animal models. Neurosci. Biobehav. Rev. 76, 235–253.
Sinclair, D., et al., 2017c. Sensory processing in autism spectrum disorders and Fragile X syndrome—from the clinic to animal models. Neurosci. Biobehav. Rev. 76, 235–253.
Talbot, Z.N., et al., 2018. Normal CA1 place fields but Discoordinated network discharge in a Fmr1-null mouse model of Fragile X syndrome. Neuron. 97 (684–697 e4).
Tallon-Baudry, C., et al., 1996. Stimulus specificity of phase-locked and non-phase-locked 40 Hz visual responses in human. J. Neurosci. 16, 4240–4249.
Van der Molen, M.J., Van der Molen, M.W., 2013a. Reduced alpha and exaggerated theta power during the resting-state EEG in Fragile X syndrome. Biol. Psychol. 92, 216–219.
Van der Molen, M.J.W., Van der Molen, M.W., 2013b. Reduced alpha and exaggerated theta power during the resting-state EEG in fragile X syndrome. Biol. Psychol. 92, 216–219.
Van der Molen, M.J.W., et al., 2010. Profiling Fragile X syndrome in males: strengths and weaknesses in cognitive abilities. Res. Dev. Disabil. 31, 426–439.
Van der Molen, M.J.W., et al., 2012. Auditory change detection in Fragile X syndrome males: a brain potential study. Clin. Neurophysiol. 123, 1309–1318.
Vasa, R.A., et al., 2016. The disrupted connectivity hypothesis of autism spectrum disorders: time for the next phase in research. Biol. Psychiatry Cogn. Neurosci. Neuroimag. 1, 245–252.
Wang, J., et al., 2013. Resting state EEG abnormalities in autism spectrum disorders. J. Neurodev. Disord. 5, 24.
Wang, J., et al., 2017. A resting EEG study of neocortical hyperexcitability and altered functional connectivity in Fragile X syndrome. J. Neurodev. Disord. 9, 11.
Wen, T.H., et al., 2018. Genetic reduction of matrix metalloproteinase-9 promotes formation of perineuronal nets around Parvalbumin-expressing interneurons and normalizes auditory cortex responses in developing Fmr1 Knock-out mice. Cereb. Cortex 28, 3951–3964.
Wen, T.H., et al., 2019. Developmental changes in EEG phenotypes in a mouse model of Fragile X syndrome. Neuroscience. 398, 126–143.
Wisniewski, K.E., et al., 1991. The fra(X) syndrome: neurological, electrophysiological, and neuropathological abnormalities. Am. J. Med. Genet. 38, 476–480.
Yu, S., et al., 1991. Fragile X genotype characterized by an unstable region of DNA. Science. 252, 1179–1181.